A Sequential Targeting Strategy Interrupts AKT-Driven Subclone-Mediated Progression in Glioblastoma

Sied Kebir[1,2,3,4], Vivien Ullrich[1,2,4], Pia Berger[1,2,4,5], Celia Dobersalske[1,2,4,5], Sarah Langer[1,2,4], Laurèl Rauschenbach[1,2,4,6], Daniel Trageser[7,8], Andreas Till[7], Franziska K. Lorbeer[7], Anja Wieland[7], Timo Wilhelm-Buchstab[9], Ashar Ahmad[10], Holger Fröhlich[10,11], Igor Cima[1,2,4], Shruthi Prasad[1,2,4,5], Johann Matschke[12], Verena Jendrossek[12], Marc Remke[2,13], Barbara M. Grüner[2,14], Alexander Roesch[2,4,15], Jens T. Siveke[2,4,16,17], Christel Herold-Mende[18], Tobias Blau[19], Kathy Keyvani[19], Frank K.H. van Landeghem[20], Torsten Pietsch[20], Jörg Felsberg[21], Guido Reifenberger[2,21], Michael Weller[22], Ulrich Sure[2,4,6], Oliver Brüstle[7,8], Matthias Simon[23,24], Martin Glas[1,2,3,4], and Björn Scheffler[1,2,4,5,25]

ABSTRACT

Purpose: Therapy resistance and fatal disease progression in glioblastoma are thought to result from the dynamics of intra-tumor heterogeneity. This study aimed at identifying and molecularly targeting tumor cells that can survive, adapt, and subclonally expand under primary therapy.

Experimental Design: To identify candidate markers and to experimentally access dynamics of subclonal progression in glioblastoma, we established a discovery cohort of paired vital cell samples obtained before and after primary therapy. We further used two independent validation cohorts of paired clinical tissues to test our findings. Follow-up preclinical treatment strategies were evaluated in patient-derived xenografts.

Results: We describe, in clinical samples, an archetype of rare ALDH1A1+ tumor cells that enrich and acquire AKT-mediated drug resistance in response to standard-of-care temozolomide (TMZ). Importantly, we observe that drug resistance of ALDH1A1+ cells is not intrinsic, but rather an adaptive mechanism emerging exclusively after TMZ treatment. In patient cells and xenograft models of disease, we recapitulate the enrichment of ALDH1A1+ cells under the influence of TMZ. We demonstrate that their subclonal progression is AKT-driven and can be interfered with by well-timed sequential rather than simultaneous antitumor combination strategy.

Conclusions: Drug-resistant ALDH1A1+/pAKT+ subclones accumulate in patient tissues upon adaptation to TMZ therapy. These subclones may therefore represent a dynamic target in glioblastoma. Our study proposes the combination of TMZ and AKT inhibitors in a sequential treatment schedule as a rationale for future clinical investigation.

Introduction

Patients with glioblastoma receiving standard-of-care treatment almost always experience disease progression under primary therapy that is surgery and combined radiotherapy (RT)- and temozolomide (TMZ)-based chemotherapy (RT/TMZ; ref. 1). Research on mechanisms of RT and TMZ resistance is rapidly progressing (e.g., refs. 2–5), but there is little evidence for improvement of clinical outcome in the care of glioblastoma relapse (6, 7). Longitudinal heterogeneity of potential cellular targets in recurrent versus primary tumor tissue is a known

[1]DKFZ-Division Translational Neurooncology at the WTZ, DKTK Partner Site, University Hospital Essen, Essen, Germany. [2]German Cancer Consortium (DKTK). [3]Division of Clinical Neurooncology, Department of Neurology, University Hospital Essen, Essen, Germany. [4]West German Cancer Center (WTZ), University Hospital Essen, Essen, Germany. [5]German Cancer Research Center (DKFZ), Heidelberg, Germany. [6]Department of Neurosurgery and Spine Surgery, University Hospital Essen, Essen, Germany. [7]Institute of Reconstructive Neurobiology, University of Bonn Medical Faculty & University Hospital Bonn, Bonn, Germany. [8]LIFE & BRAIN GmbH, Cellomics Unit, Bonn, Germany. [9]Department of Radiology, University of Bonn Medical Center, Bonn, Germany. [10]Bonn-Aachen International Center for IT (B-IT), University of Bonn, Bonn, Germany. [11]Department of Bioinformatics, Fraunhofer SCAI, Schloss Birlinghoven, Sankt Augustin, Germany. [12]Institute of Cell Biology (Cancer Research), University Hospital Essen, Essen, Germany. [13]Pediatric Neuro-Oncogenomics, University Hospital Düsseldorf, Düsseldorf, Germany. [14]Department of Medical Oncology, West German Cancer Center, University Hospital Essen, University Duisburg-Essen, Essen, Germany. [15]Department of Dermatology, University Hospital Essen, Essen, Germany. [16]Bridge Institute of Experimental Tumor Therapy, West German Cancer Center, University Hospital Essen, Essen, Germany. [17]Division of Solid Tumor Translational Oncology, German Cancer Consortium (DKTK, Partner Site Essen) and German Cancer Research Center, DKFZ, Heidelberg, Germany. [18]Division of Neurosurgical Research, Department of Neurosurgery, University of Heidelberg, Heidelberg, Germany. [19]Institute of Neuropathology, University of Duisburg-Essen, Essen, Germany. [20]Institute of Neuropathology, University of Bonn, Bonn, Germany. [21]Institute of Neuropathology, Heinrich Heine University, Düsseldorf, Germany. [22]Department of Neurology, University Hospital and University of Zurich, Zurich, Switzerland. [23]Department of Neurosurgery, University of Bonn Medical Center, Bonn, Germany. [24]Department of Neurosurgery, Bethel Clinic, University of Bielefeld Medical Center, OWL, Bielefeld, Germany. [25]Center of Medical Biotechnology (ZMB), University Duisburg-Essen, Essen, Germany.

M. Glas and B. Scheffler contributed equally as co-last authors of article.

Corresponding Author: Björn Scheffler, Professor for Translational Oncology, DKFZ-Division of Translational Neurooncology at the West German Cancer Center (WTZ), DKTK Partner Site, University Hospital Essen, University Duisburg-Essen, Hufelandstraße 55, WTZ-F, UG 01.041, Essen D-45147, Germany. Phone: 49 (0)201-723-8130; Fax: 49 (0)201-723-6752; E-mail: b.scheffler@dkfz-heidelberg.de

Clin Cancer Res 2023;29:488–500

doi: 10.1158/1078-0432.CCR-22-0611

Translational Relevance

Molecular evidence for oligoclonal trajectories and expansion of tumor cells under the influence of primary therapy has recently been discovered in glioblastoma. Here, we portray the dynamic phenotype of such a population during therapy and we underline the need for sequential molecular targeting, not yet considered in the primary clinical care of glioblastoma.

phenomenon (8) and there is evidence for subclonal trajectories in the progress towards clinical relapse (cR). Bulk sequencing of paired tissue, obtained before and after primary therapy, reveals oligoclonal regrowth patterns without a stereotype of recurrence-specific gene alterations (9–11). This challenges the view of ongoing genetic evolution as a primary cause of resistance at relapse, despite some evidence that TMZ itself might contribute to resistance by selecting for specific protein activities, e.g., involved in AKT signaling (11, 12).

To further elucidate the cellular dynamics of intra-tumor progression and to define rational targeting strategies at glioblastoma relapse, this study relied on the use of paired clinical samples representing the status of treatment-naïve primary disease and the posttreatment relapse status of the same patient. Discovery, exploration, and validation of respectively paired data suggests an enrichment and AKT-based acquired resistance in subclonal ALDH1A1+ cell hierarchies that appears to be specifically an adaptation to TMZ exposure. We here show the consequent resilience to further TMZ and that henceforth subclonal progression can be interrupted, in preclinical models, by sequential inhibition of AKT providing a yet unconsidered functional targeting approach for future clinical exploration.

Materials and Methods

Research samples

Prospectively collected tumor tissue of patients with isocitrate dehydrogenase wild-type (IDH^{WT}) glioblastoma at the University Bonn Medical Center was used for derivation of the vital cell samples of the 'discovery cohort' ($n = 15$ samples from $n = 7$ patients; Supplementary Table S1). The 'validation cohort' consisted of paired formalin-fixed, paraffin-embedded (FFPE) tissue from treatment-naïve and cR (following initial treatment) of $n = 38$ patients with IDH^{WT} glioblastoma (Supplementary Fig. S1). Specimens were provided by the Department of Neuropathology, University of Bonn Medical Center (patient IDs: 'BN'), the central nervous system (CNS) tumor tissue bank at the Department of Neuropathology, University Hospital Düsseldorf and the biobank of the University Hospital Essen (patient IDs: 'DE'; Supplementary Table S2). Studies were conducted in accordance with recognized ethical guidelines (Declaration of Helsinki). Respective local ethics committees (institutional review boards) approved the study; all patients provided informed written consent. Tumor classification relied on the World Health Organization guidelines from 2021 (13). The IDH mutation status was determined by IHC with an IDH-R132H–specific antibody followed by sequencing of IDH1 codon 132 and IDH2 codon 172 (14). The O6-methylguanine DNA methyltransferase (MGMT) promoter methylation status of the samples was determined by methylation-specific PCR or by pyrosequencing, according to (15, 16). The 'external reference cohort' comprised data of $n = 37$ IDH^{WT} glioblastoma patients (treatment-naïve vs. TMZ-exposed relapse) extracted from (ref. 10; see External validation of differentially regulated genes).

Candidate marker discovery and validation

Gene expression status of the 'discovery cohort' was determined at passage 6±1 applying the GeneChip Human Transcriptome Array 2.0 (Affymetrix Inc., San Diego) at the Department of Genomics, Life & Brain Center, University Bonn, Germany. Briefly, total RNA was isolated from vital cell samples using the RNeasy Mini Kit (Qiagen, Hilden, Germany). Complementary cDNA synthesis of 500 ng total RNA was performed using the Expand Reverse Transcriptase Kit including RNase Inhibitor (Roche, Basel, Switzerland). Sample preparation, hybridization, and quality control were performed according to Affymetrix's recommended protocols. Raw CEL files were imported into the Affymetrix Expression Console, and gene-level analysis was performed (NCBI/GEO accession No. GSE145128). Mapping of probesets to genes was based on the Affymetrix 'HTA-2_0.na34.hg19.transcript' annotation file. To assess differential gene expression, we used the R-package 'limma'. Candidate genes were queried for direct protein–protein interactions using the human-specific interaction database HIPPIE (17). Network layout and data visualization was performed with Cytoscape v.3.7.1 (www.cytoscape.org). Interactions with a low confidence score (<0.49) were discarded. In the resulting protein–protein interaction network, nodes represent genes, labeled nodes represent differentially regulated candidate genes (Supplementary Table S3). We analyzed paired RNA expression data of 37 patients with IDH^{WT} glioblastoma derived at tumor diagnosis and first tumor relapse (GLASS cohort; ref. 10). We selected the 175 genes identified on the basis of known association with TMZ treatment resistance, from pathways involved in stemness, DNA repair, and AKT signaling. Eight of the genes were differentially regulated by three criteria: (i) Statistically significant difference (FDR < 5%); (ii) Mean fold change (mFC) was > 2 or < −2; (iii) More than 2-fold differentially regulated in the same direction in at least 9 sample pairs.

Gene set enrichment analysis

Differentially enriched gene sets derived from comparing microarray gene expression data of relapse cells (TMZ→eR or cR) and treatment-naïve cells of the 'discovery cohort' were subjected to gene set enrichment analysis (GSEA; version 4.0.3 from the Broad Institute at MIT) using the MSigDB C2 database (GMT file c2.all.v6.2.symbols.gmt), 1,000 permutations, and a gene set size between 15 and 500 genes ($n = 3{,}765$ gene sets). Normalized enrichment score and FDR were used to determine statistical significance. Only gene sets with an FDR value < 0.05 ($n = 246$) were considered for further analysis.

Whole-exome sequencing

DNA isolation was performed on the 'discovery cohort' cell samples at passage 6±1 using Allprep DNA/RNA Kit (Qiagen) und Dneasy Blood & Tissue Kit (Qiagen). Library preparation on 50 ng DNA used Twist Human Core Exome Plus (Twist Bioscience). DNA sequencing was conducted on a NovaSeq 6000 system with 2×100 bp as flow cell type. Sequences with Q30 value > 93% were kept for analysis. Demultiplexing was performed with Illumina bcl2fastq (2.20), adapters were trimmed with Skewer (version 0.2.2; ref. 18). Quality trimming of the reads was not performed. DNA-Seq: Trimmed raw reads were aligned to the human reference genome (hg19) using the Burrows-Wheeler Aligner (BWA-mem version 0.7.17-cegat) and ABRA (version 2.18) for realignment of reads in target regions to facilitate accurate indel calling. In the reference hg19 the pseudoautosomal regions (PAR) on chromosome Y were masked (chrY:10001–2649520, chrY:59034050–59363566) to prevent reads that map to this region from being discarded due to mapping to two different chromosomes. Reads that aligned to more than one locus were discarded. Variant calling: A

proprietary software (CeGaT, Tübingen, Germany) was used for variant detection including variants with reasonable frequencies (observed frequency of alternative alleles from 10% upwards of sequenced reads). Variants were annotated on the basis of public data bases. Only variants with a pathogenic Functional Analysis through Hidden Markov Models (FATHMM) score were considered for further analysis (v2.3; http://fathmm.biocompute.org.uk). The quality of FASTQ files was analyzed with FastQC (version 0.11.5).

Histochemistry and immunofluorescence

Antigen labeling in FFPE tissue (4-μm sections) relied on standard protocols (**Table 1**). For permanent 3,3′-diaminobenzidine (DAB)-based labeling, automated processing was performed on the Benchmark system (Ventana Medical Systems, Roche, Mannheim, Germany). Negative controls and IgG isotype controls were processed in parallel with each batch of staining. Quantification used established methods (19). In brief, five visual fields (200x magnification) that contained the highest density of immunoreactive cells were selected for evaluation from every tissue specimen. Areas of unspecific immunoreactivity, necrosis, and macrophages were excluded. Two blinded investigators (B. Scheffler, F.K.H. van Landeghem) estimated the quantity of immunoreactive cells as a cell score (<1% = 0; 1%–5% = 1; 6%–25% = 2; 26%–50% = 3; > 50% = 4) avoiding areas of unspecific immunoreactivity, necrosis, and macrophages. Immunofluorescence (IF) analysis on deparaffinized 4-μm tissue sections used standard protocols for antigen detection, based on the conditions listed in **Table 1**. Nuclear staining was performed with Hoechst 33342 (1 μg/mL - New England Biolabs, Ipswich, MA) or with 4′,6-diamidino-2-phenylindole (DAPI)-containing mounting medium (Abcam, Cambridge, UK). A Zeiss inverted microscope was used for documentation (Zeiss, Oberkochen, Germany). Co-expression analysis for ALDH1A1 and pAKT involved paired samples from naïve versus RT ($n = 2\times12$) and paired naïve versus RT/TMZ ($n = 2\times13$) treatment conditions. Areas of vital tumor tissue and ALDH1A1+ cell accumulations were selected by two blinded investigators (D. Trageser, B. Scheffler). Ten high power fields (HPF; 400x magnification) were assessed per sample quantifying the presence and pAKT co-expression status, as well as the total number of DAPI+ nuclei (mean of 336 ± 30 ALDH1A1+ cell counts per sample). ALDH1A1/Ki67 co-expression in tumors of the BN46–patient-derived xenograft (PDX) mouse model was determined at the respective survival endpoint in four slides per condition. Six HPFs/slide were assessed for treatments with DMSO [median overall survival (mOS) = 90 days; range 87–93 days] and TMZ+MK2206 (mOS = 142 days; range: 127–148 days). Three to six HPFs/slide were quantified in TMZ-treated PDX brain samples (mOS = 124.5 days; range: 123–126). The total number of DAPI+ and co-expressing ALDH1A1+/Ki67+ cells were determined and used to calculate the relative percentage of double positive cells per HPF.

Vital cell assays

Short-term expanded vital cell populations were derived from the 'discovery cohort' of glioblastoma tissue and maintained in controlled media conditions (see below; Supplementary Table S1). *Mycoplasma*-negative status of all cultured cells were verified by standard PCR-based testing in 4-week intervals. Paired samples comprised of treatment-naïve cells from primary disease (^{naïve}cells) and cR or experimental relapse (eR) cells from the same patient. cR samples represent the status post clinical treatment (e.g., RT/TMZ). eR samples represent the status post *in vitro* exposure to TMZ (TMZ→eR) or irradiation (RT→eR). $^{TMZ\rightarrow eR}$cells were collected from regrowth of ^{naïve}cell populations following serial exposure to TMZ (500 μmol/L) for 16 days every other day. $^{RT\rightarrow eR}$cells were derived from regrowth of ^{naïve}cell populations following irradiation challenge 24 hours after plating, supplying 2 Gy ionizing irradiation daily for 12 days (6-MeV medical linear accelerator Mevatron MD2, Siemens, Munich, Germany). Recurring growth of $^{RT\rightarrow eR}$cells was noted 38±11 days after the first irradiation dose.

For data generation, vital samples were used at cell culture passages 5–12. Unless otherwise specified, cells were grown in laminin/poly-L-ornithine coated dishes in defined proliferative media containing Neurobasal, 0.5X N2 supplements, 0.5X B27 supplements, 2 mmol/L L-glutamine, and 1 μg/mL laminin (ref. 20); 20 ng/mL EGF/bFGF (R&D Systems, Wiesbaden, Germany) were provided upon plating and 10 ng/mL EGF/bFGF every other day thereafter; cell culture media, reagents, and analytical compounds were obtained from Life Technologies (Carlsbad, CA) or Sigma-Aldrich (St. Louis, MO).

In vitro drug exposure

Unless noted otherwise, vital cells were seeded 24 hours prior to drug exposure onto laminin/poly-L-ornithine coated cell culture dishes. Compounds were provided fresh with every media change and as specified in the procedures thereafter [TMZ, 500 μmol/L; N,N-diethylaminobenzaldehyde (DEAB), 50 μmol/L; MK2206, 1 μmol/L/5 μmol/L; Selleckchem, Munich, Germany]. Cell confluence was determined by software-based cell recognition (Cellavista or Nyone, Synentec, Elmshorn, Germany). AlamarBlue-based cell viability data were obtained at indicated time points as instructed by the manufacturer (Life Technologies) using a Tecan Infinite F200 instrument. For all paradigms, DMSO was applied in corresponding concentrations to control cultures. Experiments were conducted in triplicates unless noted otherwise.

Flow cytometry

For analysis, 2.5×10^5 to 5×10^5 Trypsin-dissociated (Thermo Fisher, Waltham, MA) single cells were provided with 10% FBS (HyClone, Cytiva, Marlborough, MA) centrifuged, resuspended in FACS buffer

Table 1. Antibodies and dilutions used for IHC/IF analyses.

Antigen (IHC/IF)	Company	RRID	Clone	Clonality	Host	Dilution
pAKT (Ser473)	Millipore	AB_1586879	6F5	Monoclonal	Mouse	1:200
ALDH1A1	Abcam	AB_867566	EP1933Y	Monoclonal	Rabbit	1:100
Ki67	Zytomed	N/A	K-2	Monoclonal	Mouse	1:200
HRP-linked (DAB-suited) anti-Rabbit IgG	Cell Signaling Technology	AB_2099233	–	Polyclonal	Goat	1:5,000
Anti-Rabbit IgG Alexa Fluor 555	Thermo Fisher	AB_2535849	–	Polyclonal	Goat	1:1,200
Anti-Mouse IgG Alexa Fluor 488	Thermo Fisher	AB_2534069	–	Polyclonal	Goat	1:1,200

(2 mmol/L EDTA, 0.1% BSA in 1x PBS), and incubated with human Fc Block (1:100; BD Biosciences, Franklin Lakes, NJ) for 15 minutes at room temperature. The BD Cytofix/Cytoperm Fixation/Permeabilization Kit was used (BD Biosciences) according to the manufacturer's protocol. Conjugated antibodies were used for labeling (**Table 2**). Incubation of antibodies was performed for 30 minutes on ice. Prior to the analysis, cells were washed and resuspended in FACS buffer. Samples were assayed on a FACSCelesta Flow Cytometer (BD Biosciences) using the FACSDiva software version v8.0.1.1 (BD Biosciences) and data analysis was performed using the FlowJo software version v10.5.3 (BD Biosciences). Unless mentioned otherwise, experiments were conducted in triplicates. The Aldehyde Dehydrogenase assay was performed using the ALDEFLUOR Assay Kit (STEMCELL Technologies, Vancouver, CA) as using manufacturer conditions. $ALDH^{br}$ cells were quantified on a FACSCalibur or a FACSCanto II system (BD Biosciences) and analyzed by FlowJo according to manufacturer suggestions with DEAB reagent as a negative control.

Protein expression analysis

Thirty microgram of total protein was separated by SDS-PAGE and transferred onto nitrocellulose membranes (Sigma-Aldrich) by electroblotting. Membranes were blocked in 5% milk powder (Carl Roth GmbH, Karlsruhe, Germany) and TBS with 0.05% TWEEN-20 (Carl Roth GmbH) for 1 hour, supplied with primary antibodies overnight at 4°C or for 1 hour at room temperature (β-actin, Sigma- Aldrich) and detected with a horseradish peroxidase (HRP)-coupled secondary antibody using Luminata HRP Substrate (Burlington, MA) and the ChemiDoc System (Bio-Rad, Hercules, CA; **Table 3**). Intensity quantification was performed using ImageJ software.

Knockdown and overexpression studies

Knockdown experiments were performed using a MISSION short hairpin RNA (shRNA) plasmid against ALDH1A1 and a non-targeting control (Sigma-Aldrich) by lentiviral transduction. Lentiviruses were produced in 293FT cells using packaging reagents following the manufacturer's instructions (Sigma-Aldrich). For overexpression, coding sequences of ALDH1A1 or control-GFP were cloned into pLenti6.2/V5-DEST Gateway Vector (Life Technologies). Transduced cells were selected for up to 2 weeks with blasticidin (5 μg/mL; Santa Cruz Biotechnology). Stable expression/knockdown was confirmed by Western blots or by qPCR using standard protocols and the following primer sequences: ALDH1A1, GGACCAGTGCAGCAAATCAT (forward), TACCACGCCATAGCAATTCA (reverse); GAPDH, CTGCTTTTAACTCTGGTAAAGT (forward), GCGCCAGCATCGCCCCA (reverse). For transient, siRNA-based inhibition of ALDH1A1 expression, 10,000 cells/cm^2 were seeded in ABX-free media one day prior to siRNA transfection. The transfection was performed using Lipofectamine RNAiMAX Transfection Reagent (Thermo Fisher), Opti-MEM Reduced Serum Medium (Thermo Fisher), 5x siRNA buffer (Dharmacon, Lafayette, CO), and the specific siRNAs (20 μmol/L): ON-TARGETplus Non-targeting Pool (5 nmol; D-001810–10–05) and ON-TARGETplus Human ALDH1A1 (216) siRNA – SMARTpool (5 nmol; L-008722–00–0005), both from Horizon Discovery (Waterbeach, UK). After 5 days, cells were seeded for neurosphere formation as described below and an additional siRNA transfection was performed while plating. The siRNA knockdown was confirmed by qPCR using standard protocols and the following primer sequences: ALDH1A1, GCACGCCAGACTTACCTGTC (forward), CCTCCTCAGTTGCAGGATTAAAG (reverse); RPL37A, GACGTACAATACCACTTCCGC (forward), GGAGCGTCTACTGGTCTTTCA (reverse).

Limiting dilution analysis

0.5 cells/well were seeded in five 96-well plates. Using automated software-based cell recognition (Nyone) the distribution of single cells/well was subsequently confirmed. After 16 days of expansion, the developed colonies and cells were photodocumented for each colony and counted.

Neurosphere assay

Similar to described conditions for the assay (20–22), single-cell suspensions of 5×10^5 cells/cm^2 were plated in 1:1 Methylcellulose (Sigma-Aldrich)/proliferative media, provided with 20 ng/mL EGF/bFGF, and inoculated into nonadhesive culture dishes. 10 ng/mL EGF/bFGF was added every other day thereafter. At 12 days, first-generation (1°) neurospheres were documented (Nyone) and quantified. From these, a single-cell suspension was plated under identical conditions for analysis of second-generation (2°) neurospheres on day 24 of the assay. To evaluate for generation of neuronal and glial phenotypes, a representative fraction of 2° neurospheres was plated onto laminin/poly-L-ornithine coated dishes and, after attachment, provided with proliferative media devoid of mitogens to allow differentiation for 2 weeks. Samples were then fixed (ROTIHistofix, 4%) and processed for standard IF analysis using the antibodies and dilutions listed in **Table 4**. Cells were mounted using Aqueous Fluoroshield mounting medium (Abcam) and imaged on a Zeiss inverted microscope. Experiments were conducted in triplicates.

Orthotopic xenografts

Animal studies were approved by regulatory authority (LANUV#84–02.04.2014.a316). 10-week-old Fox Chase SCID/beige mice (Charles River, Germany) were engrafted with $1 \times 10^{6\ naïve}$BN46 cells, unilaterally injected into the right striatum (0.7 mm anterior to the bregma, 2.6 mm lateral from the midline, at a depth of 3.0 mm). Drug regimens were initiated at day 60 posttransplantation. Mice received TMZ (50 mg/kg, i.p.; 5 days per week), MK2206 (100 mg/kg,

Table 2. Antibodies and dilutions used for flow cytometry analyses.

Antibody (FACS)	Conjugation	Company	RRID	Clone	Dilution
Human Fc block	–	BD Biosciences	AB_2869554	Fc1.3216	1:100
ALDH1A1	FITC	Abcam	N/A	03	1:5
pAKT (pS473)	PE	BD Biosciences	AB_1645328	M89–61	1:2.5
Active caspase-3	FITC	BD Biosciences	AB_397234	C92–605	1:5
ALDH1A1	–	Abcam	AB_867566	EP1933Y	1:100
Human IgG1 isotype control	FITC	BioLegend	AB_2847831	QA16A12	1:25
Mouse IgG1, κ isotype control	PE	BioLegend	AB_326435	MOPC-21	1:500
Sec. antibody goat anti-rabbit	Alexa Fluor 555	Life Technologies	AB_2535849		1:200

Table 3. Antibodies and dilutions used for Western blots (WB).

Antigen (WB)	Company	RRID	Clone	Clonality	Host	Dilution
ALDH1A1	Abcam	AB_867566	EP1933Y	Monoclonal	Rabbit	1:2,000
PTEN	DAKO	AB_2174185	6H2.1	Monoclonal	Mouse	1:100
pAKT	Cell Signaling	AB_2315049	D9E	Monoclonal	Rabbit	1:1,000
pGSK3β	Cell Signaling	AB_10013750	D85E12	Monoclonal	Rabbit	1:1,000
β-Actin	Sigma	AB_476744	AC-15	Monoclonal	Mouse	1:10,000
HRP-linked anti-mouse IgG	Cell Signaling	AB_330924	–	–	Goat	1:5,000
HRP-linked anti-rabbit IgG	Cell Signaling	AB_2099233	–	–	Goat	1:5,000

orally, 6 times once every other day) or control solvent (DMSO in PBS); as specified. For TMZ→TMZ/MK2206, mice were first treated with TMZ alone (50 mg/kg, i.p.; 5 days/week) for 3 weeks. Subsequently, TMZ was administered alternating with MK2206 (100 mg/kg, orally; 6 times every other weekday) before mice continued to receive TMZ-only (50 mg/kg, i.p.; 5 days/week). Alternatively, for TMZ/MK2206→TMZ, mice were treated with alternating TMZ and MK2206 for 2 weeks, followed by TMZ-only (5 days/week). Mice were monitored daily and euthanized in the event of clinical deterioration (when neurologic symptoms such as hemiparesis or gait disorder developed or significant weight loss occurred, defined as the loss of > 25% of pretreatment body weight).

Statistical analysis

Unless otherwise specified, data are presented as mean ± SD. Statistical methods, including corrections for multiple testing are described in each set of data. The significance threshold was set at 0.05. R (The R Foundation for Statistical Computing, v4.1.3) and GraphPad Prism v8 software was used for data analysis and visualization.

Data availability

The genomic sequencing data have been deposited at NCBI/GEO under the accession no. GSE145128. All computational structural information is available upon reasonable request.

Results

Discovery of ALDH1A1 subclonal enrichment

Building on previous strategies to study subclonal dynamics *ex vivo* (22), we generated a 'discovery cohort' from $n = 7$ patients with glioblastoma (IDH^{WT}; Supplementary Table S1). The cohort consisted of primary cells isolated from treatment-naïve tissue at initial diagnosis (^{naïve}cells; $n = 7$) paired with primary cells that were generated from relapse surgery of the same patients after clinical RT/TMZ treatment (^{cR}cells; $n = 5$). In two cases, where relapse tissue was not available, and in one index case (BN118), paired eR cells were generated by serially exposing ^{naïve}cells to TMZ *in vitro* ($^{TMZ\rightarrow eR}$cells; $n = 3$; **Fig. 1A**). A comparative analysis of transcriptomes derived from these paired samples ($n = 15$) uncovered the expression of 175 potential markers linked to drug resistance, of which eight were differentially expressed (**Fig. 1B**; Supplementary Table S3). The differential expression of the top upregulated gene *ALDH1A1* (mFC, +6.3) could be validated, among the 175 tested, on a cohort of publicly available RNA sequencing data of paired treatment-naïve and RT/TMZ relapse glioblastoma tissue samples (ref. 10; **Fig. 1C**). We next studied ALDH1A1 expression by IHC in FFPE tissue from an independent 'validation cohort' of $n = 38$ patients with glioblastoma with available paired primary and relapse tissues (IDH^{WT}; Supplementary Figs. S1 and S2). Initial treatment of these patients consisted of surgery and either RT/TMZ or radiotherapy-alone (RT-only; Supplementary Table S2). In these samples, we observed distinctive patterns of subclonal enrichment. At primary disease, ALDH1A1+ cells were faintly stained and sparsely dispersed within the tumor. By contrast, focal accumulations of strongly immunoreactive ALDH1A1+ cells were evident in RT/TMZ relapse tissues (**Fig. 1D**), but not in RT-only relapse tissues (**Figs. 1E** and **F**). This finding indicated a relationship between clinical TMZ exposure and the expansion of a putatively clonal ALDH1A1+ cell population in progressing glioblastoma.

Assessment of ALDH1A1+ cells from treatment-naïve primary disease

ALDH1A1 has frequently been described as a marker for stemness in human cancers (23), even though early investigations found it dispensable for stem cell function in murine hematopoietic and nervous systems (24). Studies on human glioblastoma cell lines suggested the enzyme as a mediator of TMZ resistance (25). Yet, ALDH1A1 immunoscoring in glioma/glioblastoma tissue from cohorts of primary disease inconsistently predicted patient survival (26, 27). To further explore the role of ALDH1A1 under TMZ subclonal selection pressure, we performed a series of genetic and pharmacologic interference assays *in vitro*.

Table 4. Antibodies and dilutions used for neurosphere IF analyses.

Antigen	Company	RRID	Clone	Clonality	Host	Dilution
GFAP	Dako	AB_10013382	–	Polyclonal	Rabbit	1:400
Tubulin β3 (TUBB3)	Covance/BioLegend	AB_2313773	TUJ1	Monoclonal	Mouse	1:1,000
Anti-Rabbit IgG Alexa Fluor 555	Thermo Fisher	AB_2535849	–	Polyclonal	Goat	1:800
Anti-Mouse IgG Alexa Fluor 488	Thermo Fisher	AB_2534069	–	Polyclonal	Goat	1:800

Abbreviation: GFAP, glial fibrillary acidic protein.

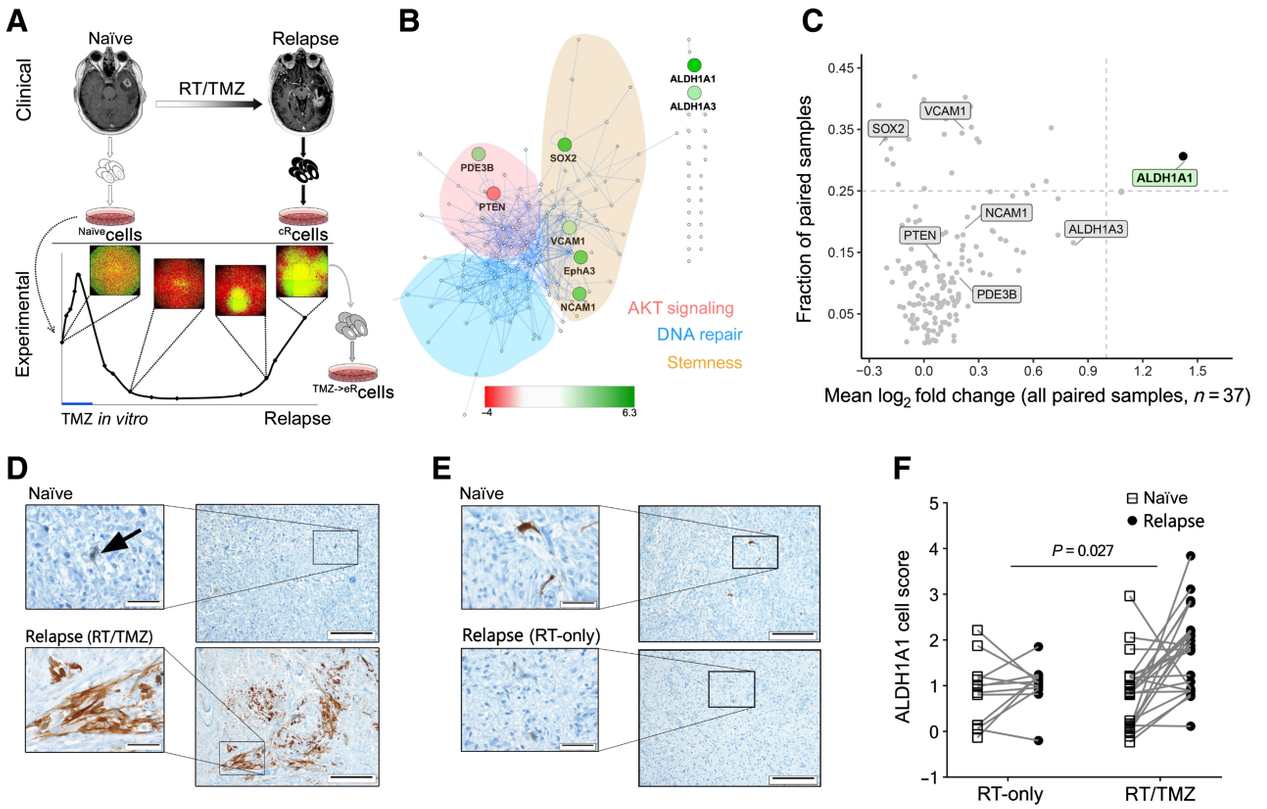

Figure 1.

Discovery of ALDH1A1 subclonal enrichment in cohorts of paired patient tissue and vital cells. **A** and **B,** Discovery cohort. **A,** Scheme illustrates derivation of tissue and primary cell samples from treatment-naïve primary disease, and from paired cR or eR. cR samples represent the status post clinical treatment (e.g., RT/TMZ). eR samples represent the status post *in vitro* exposure to TMZ (TMZ→eR) or irradiation (RT→eR, not shown). Graph depicts the generation of $^{TMZ\rightarrow eR}$cells, monitored *in vitro* by Cellavista-based false-colored cell recognition (green, cells; red, plasticware; blue bar, 16-day exposure to 500 μmol/L TMZ; endpoint, 60 days). **B,** Network represents protein interactions of 175 candidate genes using the HIPPIE database. Colored areas denote functional categories. Differential expression of selected genes from the discovery cohort are represented as mFC from −4.0 (red) to +6.3 (green). **C,** Plot represents differential gene expression of 175 candidate genes within a set of paired tissue samples from $n = 37$ patients with IDH^{WT} glioblastoma (reference cohort; ref. 10). Dashed lines represent thresholds used to select differentially expressed genes (Methods; Supplementary Table S3). **D,** Representative ALDH1A1 IHC images of paired glioblastoma tissue samples before and after clinical RT/TMZ therapy. Arrow: ALDH1A1+ cell. **E,** Representative ALDH1A1 IHC images of paired glioblastoma tissue samples before and after clinical RT-only. Blue, hematoxylin counterstain; brown, permanent diaminobenzidine reaction for ALDH1A1. Scale bars (**D**, **E**): 200 μm (overviews) and 50 μm (insets). **F,** Graph represents ALDH1A1+ cell frequencies in glioblastoma tissue scored from IHC (< 1% = 0; 1%–5% = 1; 6%–25% = 2; 26%–50% = 3; > 50% = 4) in paired naïve versus relapse glioblastoma tissue sections. Primary clinical treatment involved either RT-only or combined RT/TMZ (Supplementary Table S2). *P* value by Fisher exact test.

We first noted that serial exposure of ^{naïve}cells to TMZ (generating $^{TMZ\rightarrow eR}$cells) resulted in increased ALDH-bright ($ALDH^{br}$) cell frequencies and ALDH1A1 protein levels in eR cell populations. For example, in the $^{TMZ\rightarrow eR}$BN46 model, the $ALDH^{br}$ cell fraction increased from means of 6% (^{naïve}BN46) to 55%, accompanied by a 37-mFC of ALDH1A1 in the flow cytometry analysis (**Fig. 2B**; Supplementary Fig. S2B). This effect could not be observed upon serial *in vitro* exposure to ionizing irradiation (resulting in $^{RT\rightarrow eR}$cells, see Methods; **Fig. 2A**; Supplementary Fig. S2A). These data further indicated that the observed increase of ALDH1A1+ cells at glioblastoma relapse may be a specific effect of TMZ.

We next tested the ^{naïve}BN46 patient cells in a protracted *in vitro* assay and observed that their recurrent growth upon TMZ exposure could be repressed by pharmacologic inhibition of ALDH with DEAB or by knockdown of *ALDH1A1* expression with shRNA (**Fig. 2C** and **D**). We speculated that, in line with the literature (25), increasing ALDH1A1 would mediate increasing TMZ resistance. In overexpression experiments, we observed that $ALDH1A1^{high\ naïve}$cells recovered up to three weeks earlier from serial TMZ exposure compared with control ^{naïve}cells transduced with green fluorescent protein (GFP Ctrl; **Fig. 2E**). However, cocultures of $ALDH1A1^{high}$ and GFP Ctrl cells (1:1 ratio) revealed similar initial drug response kinetics (**Fig. 2F**). This argued for a similar degree of TMZ sensitivity, at least during initial exposure, in both cell types and against an intrinsic TMZ resistance in treatment-naïve $ALDH1A1^{high}$ cells. Furthermore, population-based knockdown or overexpression of *ALDH1A1* in ^{naïve}BN46 patient cells did not strongly alter stemness-associated features (Supplementary Fig. S2C). Moreover, we did not observe significant effects on clonogenicity and clonal cell growth as determined by the limiting dilution assay (**Fig. 2G**; Supplementary Fig. S2D). Similarly, in the neurosphere assay, the frequency of neurosphere-forming cells (indicator for clonogenicity), the ratio between primary (1°) and secondary (2°) neurospheres (indicator for self-renewal), and the ability to generate neuronal and glial phenotypes (indicator for potency), did not vary significantly among the tested conditions (**Fig. 2H**; Supplementary Fig. S2E–S2G).

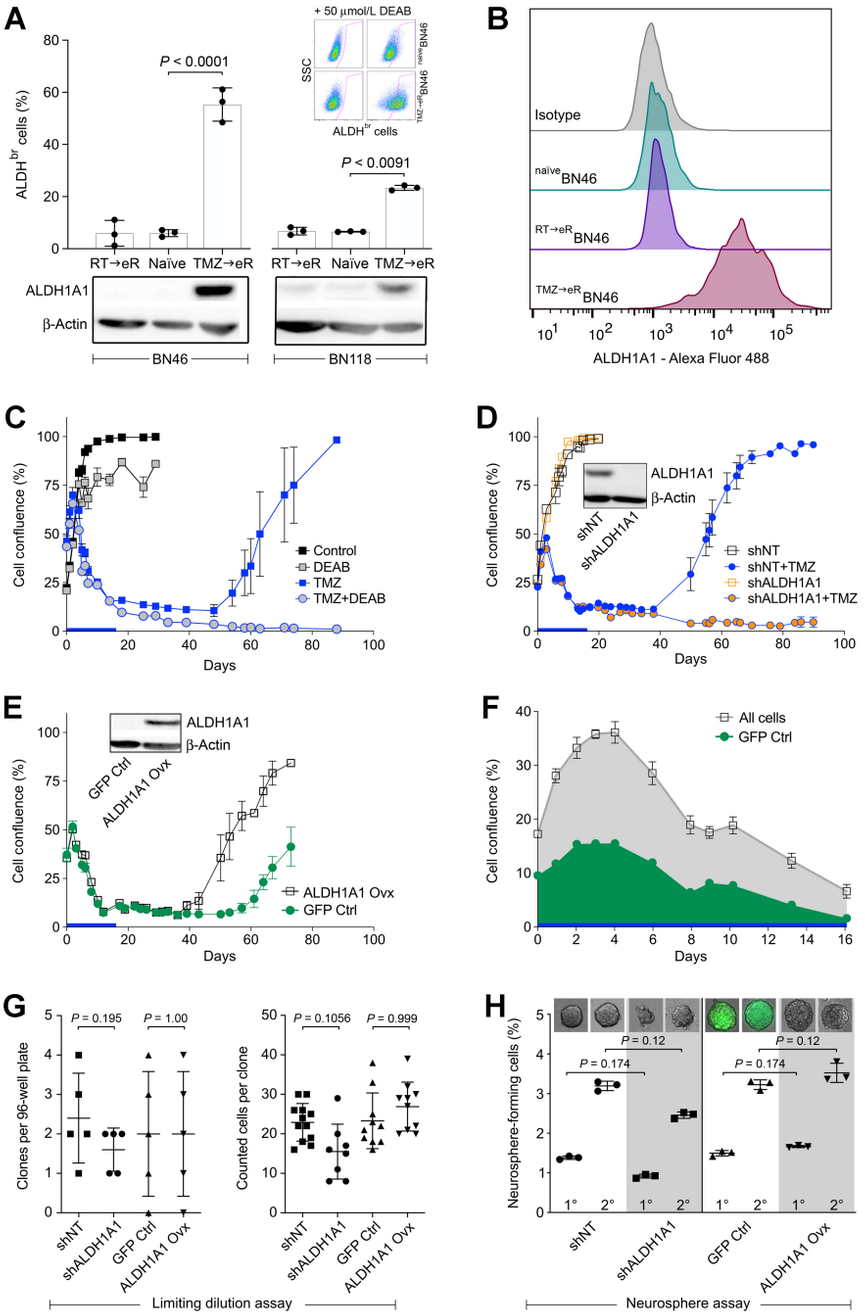

Figure 2.

Assessment of ALDH1A1+ cells from primary, treatment-naïve glioblastoma. **A,** Bar chart displays ALDEFLUOR-based quantification of ALDH-bright (ALDH^{br}) vital cells from naïve vs. eR conditions, i.e., status post *in vitro* exposure to TMZ (TMZ→eR) or irradiation (RT→eR). Two cases of patient cells shown (BN46, BN118). Data as mean ± SD. *P* values by one-way ANOVA with Tukey *post hoc* test. *Upper inset*: Representative flow cytometry profiles of BN46 cells from the assay. *Lower inset*: Western blots of respective samples. **B,** Histograms represent ALDH1A1 flow cytometry data from naïve versus eR BN46 cells. (**C–F**), Long-term, triplicate *in vitro* assays on treatment-naïve BN46 cells. In all graphs, TMZ exposure (16 days, 500 µmol/L) is shown as blue bar on the *x*-axis. Data as mean ± SEM. **C,** Dynamics of cell confluence under control conditions (0.01% DMSO) versus continuous exposure to DEAB. **D,** Dynamics of cell confluence with shRNA interference of ALDH1A1 expression. shNT, non-targeting control. *Inset*: Western blot of assayed samples. **E,** Dynamics of cell confluence upon ALDH1A1 overexpression (Ovx) GFP Ctrl, green fluorescent protein-control. *Inset*: Western blot of assayed samples. **F,** (1:1) co-culture of ALDH1A1 Ovx/GFP Ctrl BN46 cells. Displayed are the dynamics of cell fractions during TMZ exposure (fluorescence-detected GFP-expressing Ctrl cells vs. all cells). **G,** Limiting dilution assay evaluating clonal expansion of individually plated ^{naïve}BN46 shALDH1A1 and ^{naïve}BN46 ALDH1A1 Ovx cells and their respective controls (see Supplementary Fig. S2D). The left dotplot shows counted clones, the right dotplot shows counted cells per clone at 16 days after plating. **H,** Neurosphere assay evaluating first and second neurosphere generation of ^{naïve}BN46 shALDH1A1 and ^{naïve}BN46 ALDH1A1 Ovx cells and their respective controls. Dotplot shows estimation of neurosphere-forming cell frequencies from counting generated neurospheres 12 days after seeding of cells. *Upper insets*: Phase contrast appearance of respective neurospheres. Data in **G** and **H** shown as mean ± SD. *P* values obtained by pairwise comparisons using Wilcoxon test, adjusted for multiple testing.

This set of data confirms on the one hand the association of TMZ and ALDH1A1 expression in glioblastoma, but on the other hand suggests that ALDH1A1 is not necessary to drive subclonal progression of primary disease.

AKT drives the progression of ALDH1A1+ cells in glioblastoma

Because glioblastoma stem cells have been shown to adapt under treatment (28), and in particular, ALDH1A1+ cells have been suggested to adapt in response to clinical EGFR inhibitor therapy (29), we speculated that ALDH1A1+ cells may acquire adaptive molecular features upon TMZ exposure. To test this hypothesis, we compared ALDH1A1 cells from treatment-naïve and paired relapse conditions *in vitro*.

Clinical RT/TMZ relapse cell samples demonstrated consistent, yet variably strong increases of ALDH1A1 compared with their paired ^{naïve}cell populations (**Fig. 3A**; Supplementary Fig. S3A). By flow cytometry, we determined respective mFCs of 84.0 (^{cR}BN91), 32.3 (^{cR}BN118), 0.9 (^{cR}BN123), and 2.2 (^{cR}BN132). The data distribute around the mFC of 37.0 recorded for eR $^{TMZ→eR}$BN46 cells (Supplementary Figs. S2B and S3B), which we further used as a reference for analysis. Performance of these 'naturally' ALDH1A1-enriched cR samples was then evaluated in the neurosphere assay (Supplementary

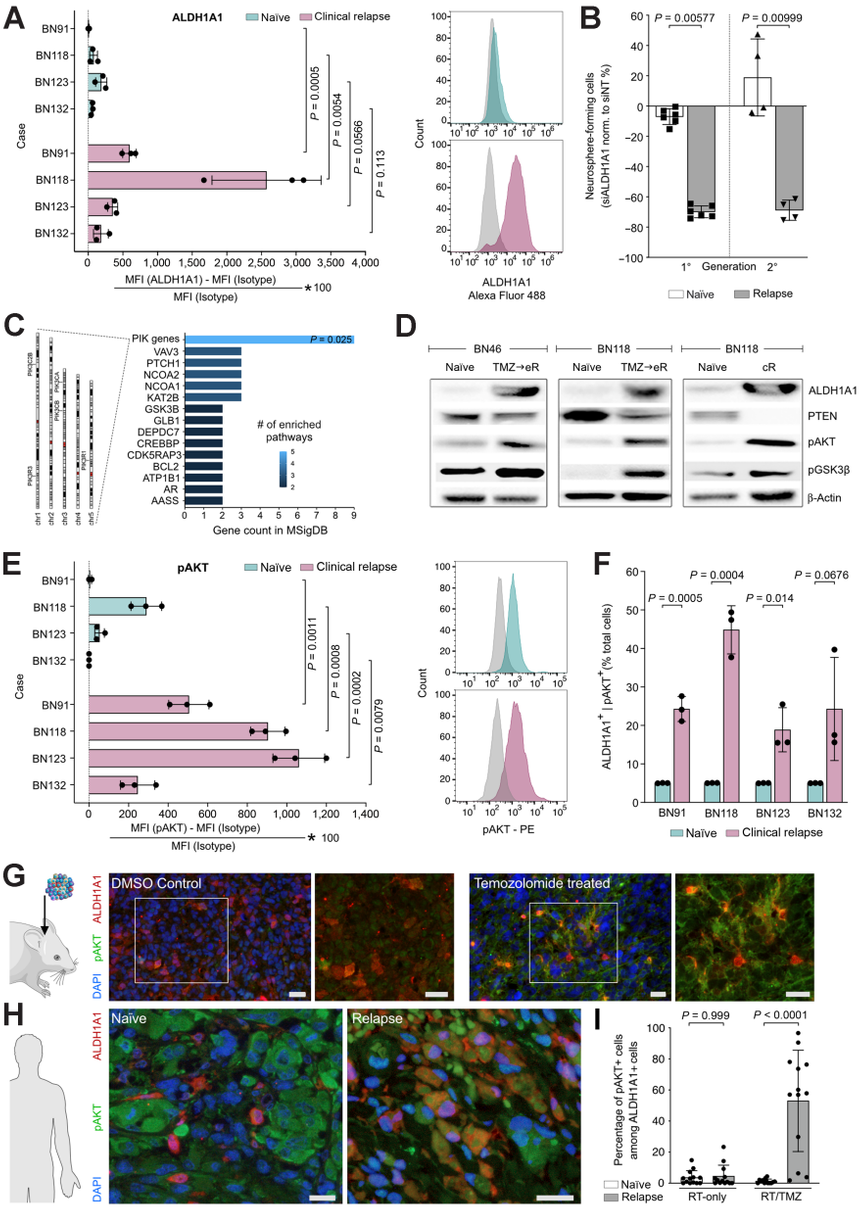

Figure 3.

AKT-driven progression of ALDH1A1+ cells in glioblastoma. **A,** Bar chart represents ALDH1A1 mean fluorescence intensities (MFI) normalized to isotype control in paired treatment-naïve versus cR patient cell samples measured by flow cytometry. Mean ± SD. *P* values obtained by pairwise comparisons using Wilcoxon test, adjusted for multiple testing. *Inset*: Representative histograms of case BN118 (gray, isotype controls). **B,** Neurosphere assay of ALDH1A1 siRNA and non-targeting control (siNT) of paired treatment-naïve versus cR cell samples (BN118, BN123; also see Supplementary Figs. 3D and E). Individual data points represent triplicates (1°) and duplicates (2°) per case. Results normalized to siNT and shown as mean ± SD. *P* values obtained by pairwise comparisons using Wilcoxon test, adjusted for multiple testing. **C,** GSEA using microarray gene expression data of experimental and cR cells (TMZ→eR and cR) and treatment-naïve cells of the "discovery cohort." The top 15 leading edge genes associated with two or more significantly enriched pathways are displayed. *P* value calculated by Fisher exact test. **D,** Protein expression patterns in paired primary cell samples determined by Western blot. **E,** Bar chart represents pAKT (Ser473) MFI normalized to isotype control in paired treatment-naïve versus cR patient cell samples measured by flow cytometry. Mean ± SD. *P* values obtained by pairwise comparisons using Wilcoxon test, adjusted for multiple testing. *Inset*: Representative histograms of case BN118 (gray, isotype control). **F,** Bar chart showing percent ALDH1A1/pAKT (Ser473) co-expressing cells as determined by flow cytometry in paired samples (treatment-naïve vs. cR; see Supplementary Fig. S3I). Data shown as mean ± SD, *P* values calculated using a Kruskal–Wallis test followed by Dunn *post hoc* test. **G,** Representative IF images of pAKT (Ser473) and ALDH1A1 of ^{naïve}BN46 orthotopic xenografts from mice treated with DMSO (OS = 93 days) and TMZ (OS = 126 days). Respective treatment schedules in **Figure 4J**. Scale bars: 20 μm. **H,** Representative IF of pAKT (Ser473) and ALDH1A1 in paired patient glioblastoma tissue before (at primary disease, treatment-naïve) and after clinical RT/TMZ (at glioblastoma relapse). Scale bars: 20 μm. **I,** Barplot showing frequencies of ALDH1A1+/pAKT (Ser473)+ cells counted in paired glioblastoma tissues of the validation cohort (Supplementary Fig. S1). Primary clinical treatment involved either RT-only or combined RT/TMZ (Supplementary Table S2). Data displayed as mean ± SD, *P* values obtained by one-way ANOVA with Tukey *post hoc* test.

Figs. S3C and S3D). We noted that knockdown of *ALDH1A1* in ^{cR}BN118 and ^{cR}BN123 cells resulted in a uniformly strong decrease of clonogenic activity, by 70%±4% and 69%±7% for 1° and 2° neurospheres, which is in strong contrast to the almost unchanged activity after knockdown of *ALDH1A1* in the paired treatment-naïve samples (**Fig. 3B**). Similarly, for the $^{TMZ\rightarrow eR}$BN46 cells, knockdown of *ALDH1A1* reduced 1° and 2° neurospheres by 48%±2% and 56%±7% respectively, while the clonogenic activity of the parental ^{naïve}BN46 cells remained hardly affected (Supplementary Figs. S3D and SD3E). These data further supported the hypothesis that exposure of TMZ leads to an enrichment of ALDH1A1+ cells characterized by altered functional activity.

To discover potential underlying mechanisms, we used GSEA on the paired expression data of the 'discovery cohort' revealing PI3K–AKT pathway genes more frequently enriched across the leading edges of all significantly enriched pathways (**Fig. 3C**). To test if this enrichment underlies genetic events, we analyzed single nucleotide variants in the paired samples using whole-exome sequencing. FATHMM, retaining all variants documented as pathogenic with a major allele frequency of at least 10%, did not reveal significant differences in the mutational profile of relevant PI3K–AKT pathway driver genes in treatment-naïve versus relapse samples ($P = 0.9743$; Supplementary Table S4). However, we did observe increased pathway activity demonstrated in paired ^{naïve}cells vs. experimental and cR samples by Western blot and flow cytometry (**Fig. 3D** and **E**; Supplementary Figs. S3F and S3G). In particular, pAKT+/ALDH1A1+ double-positive cells represented only 5%±0.04% of the treatment-naïve cells and up to 49% (mean 28%±13%) of the total cell population in the paired cR samples. This subclonal enrichment was consistent in 4 of 4 pairs of naïve versus clinical RT/TMZ relapse samples with mFCs of 3.8 (^{cR}BN91), 7.9 (^{cR}BN118), 2.8 (^{cR}BN123), and 3.8 (^{cR}BN132; **Fig. 3F**; Supplementary Fig. S3H) and in naïve versus eR cells ($^{TMZ\rightarrow eR}$BN46; mFC = 3.1; Supplementary Figs. S3I and S3J), but not in *in vitro* exposed naïve cells to ionizing irradiation (Supplementary Fig. S3J). Furthermore, the emergence of pAKT+/ALDH1A1+ cellular enrichment could be verified as well in TMZ-treated tumor xenografts (**Fig. 3G**) and in original patient tissue (**Fig. 3H**). IF analysis of FFPE specimens of the 'validation cohort' (**Fig. 3H** and Supplementary Table S2) revealed in the treatment-naïve as well as in the paired clinical RT-only relapse tumor tissue, rare ALDH1A1+ cells intermixed with heterogeneously distributed pAKT+ cells. By contrast, we noted characteristic clusters formed by abundantly co-expressing ALDH1A1+/pAKT+ cellular phenotypes in the paired clinical RT/TMZ relapse tissue, but only few in the RT-only relapse tissue (**Fig 3I**), indicating that this effect was specific to TMZ.

pAKT is known for its heterogeneous distribution in human glioblastoma (30) and there is a large body of evidence on glioblastoma-promoting AKT activity (31). Early research had already suggested an involvement of AKT in stem-like properties of cancer cells and during glioma formation (32, 33). A subclonally confined process of aberrant AKT signaling that evolves dynamically under TMZ exposure from primary disease towards glioblastoma relapse has hitherto not been described.

Targeting of AKT-driven subclonal progression of ALDH1A1+ cells

To explore drug targeting under this premise, we tested the clinical-grade allosteric AKT inhibitor MK2206 (34) *in vitro*, in a paradigm involving continuous TMZ exposure (**Fig. 4A**). TMZ resistance levels were consistently increased in the (TMZ preexposed) experimental and cR cells vs. their paired treatment-naïve samples, as quantified by read-out of cell confluence and viability on days 8 and 10, respectively (**Fig. 4B** and **C**). Combinatorial application of MK2206 (5 μmol/L) did not alter the sensitivity of treatment-naïve cells to TMZ, but it efficiently reverted the high levels of TMZ resistance in relapse cells to the more sensitive status of paired treatment-naïve cells (Supplementary Fig. S4A). Intriguingly, we noted that the combinatorial application of MK2206 *in vivo* also reverted the increasing levels of proliferative activity in ALDH1A1+ cells characteristically observed in TMZ-treated tumor xenografts (**Fig. 4D** and **E**; Supplementary Fig. S4B). This correlated with increasing levels of active caspase-3, a classic apoptosis marker (ref. 35; **Fig. 4F**). Notably, the pro-apoptotic effect of MK2206 + TMZ in relapse cells even appeared to exceed the antitumor effects that TMZ-alone had in treatment-naïve cell samples (**Fig. 4G**). And, in line with the hypothesis of an AKT-driven subclonal progression of ALDH1A1+ cells, we observed that the application experiments of MK2206 + TMZ targeted the vast majority of ALDH1A1+ cells within the experimental and cR cell populations (**Fig. 4H**; Supplementary Fig. S4A).

On the basis of the collective findings of our study, we next designed a rational targeting strategy for ALDH1A1+ glioblastoma cells. To interfere with the dynamics of ALDH1A1+ subclonal progression, we assayed TMZ and MK2206 in the long-term *in vitro* approach originally used to generate experimental $^{TMZ\rightarrow eR}$cells. We observed that MK2206 alone did not inhibit cellular proliferation, it rather prevented eR when applied subsequently to TMZ exposure *in vitro* (**Fig. 4I**). Sequential treatment was therefore modeled in follow-up xenograft experiments. Schedules were initiated in SCID/beige mice at day 60 after orthotopic implantation of ^{naïve}BN46 cells, corresponding to 67% of the vehicle control mOS time (DMSO = 90 days; **Fig. 4J**; Supplementary Fig. S4C). MK2206 monotherapy did not alter survival, but TMZ did, in line with clinical expectations [mOS (TMZ) = 112 days; mOS (DMSO vs. TMZ), $P = 0.0005$]. The combination of MK2206, within the first 2 weeks of TMZ treatment, did not have an added benefit. However, delayed addition of MK2206, during weeks 4 to 5, of TMZ exposure extended survival significantly [mOS (TMZ→TMZ/MK2206) = 136 days; mOS (TMZ vs. TMZ→TMZ/MK2206), $P < 0.0001$; **Fig. 4D**]. In summary, these results showed that the appropriately timed treatment sequences of TMZ + MK2206 yielded a > 2-fold survival benefit over the already effective TMZ monotherapy, illustrating a sequential targeting paradigm for rational interference with AKT-driven subclonal progression in glioblastoma (**Fig. 4K**).

Discussion

TMZ-based treatment schemes represent a cornerstone of the primary care measures in glioblastoma (1). Resistance to TMZ is considered the limiting factor of effective therapy; a variety of mechanisms and molecular constellations (e.g., an unmethylated MGMT promotor status) likely contribute to resistance of tumor cells against the actions of this chemotherapeutic (5). Restricted populations of preexisting glioma stem cells had been considered as intrinsically resistant and as drivers for progression of disease (e.g., ref. 37). It was tempting to likewise consider the rare ALDH1A1+ cells at primary disease as prototypical resistant clones, because they accumulate in paired recurring tumor tissue after clinical treatment. Our investigation could not reveal evidence for primary resistance, we instead observed that these cells can adapt, specifically to TMZ exposure, and then proliferate under the continued influence as a more TMZ resistant hierarchy, driven by aberrant AKT signaling. This occurred irrespective of the MGMT promotor status and without association of

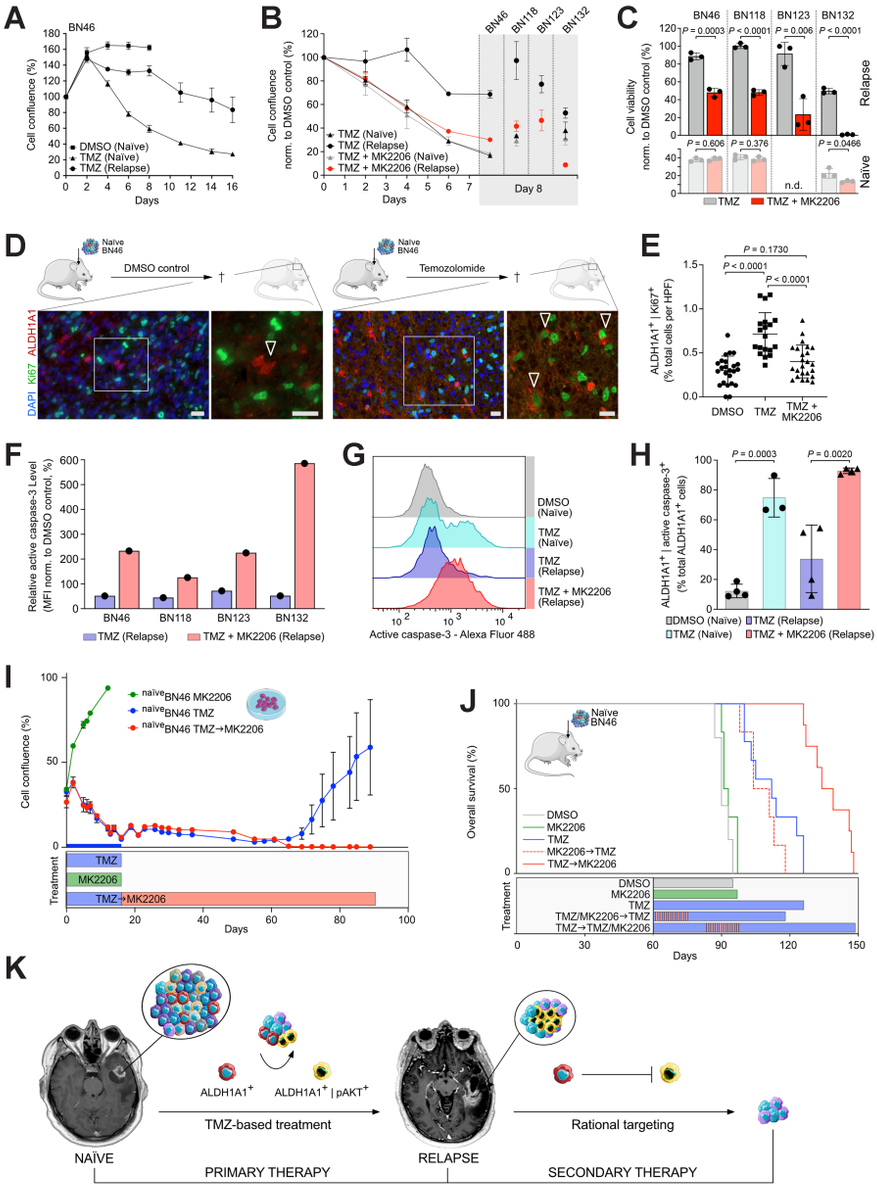

Figure 4.

Targeting of AKT-driven subclonal progression of ALDH1A1+ cells. **A,** Graph shows percent *in vitro* cell confluence of paired naïve versus eR cells (BN46) treated with control DMSO (0.05%) versus 500 μmol/L TMZ (software-based cell recognition, NyOne). Data shown as mean ± SD of $n = 3$ technical replicates. **B,** Percent *in vitro* cell confluence of cells derived from paired naïve versus eR (BN46) or naïve versus cR samples (BN118, BN123, BN132) treated with TMZ (500 μmol/L) versus TMZ (500 μmol/L) + MK2206 (5 μmol/L). Data normalized to DMSO-control and shown as mean ± SD, $n = 3$ technical replicates, NyOne-readout on day 8 (Supplementary Fig. S4A). **C,** Bar plots show cell viability readouts on day 10 (alamarBlue) for samples described in **B**. Data were normalized to DMSO-control and shown as mean ± SD of $n = 3$ replicates. *P* values calculated by one-way ANOVA followed by Tukey *post hoc* test. **D,** Representative IF images of ALDH1A1 and Ki67 of ^{naïve}BN46 orthotopic xenografts from mice treated with DMSO (OS = 87 days) and TMZ (OS = 126 days). Arrows: ALDH1A1+/Ki67− cells (left) and ALDH1A1+/Ki67+ cells (right). Scale bars: 20 μm. **E,** Dot plot shows percent ALDH1A1+/Ki67+ cells per treatment condition in the BN46-PDX model. Treatment schedules in **J**. $n = 4$ slides per condition; DMSO-treated (24 HPFs) TMZ-treated (19 HPFs), TMZ + MK2206-treated (24 HPFs). Results as mean ± SD, *P* values calculated by one-way ANOVA followed by Tukey *post hoc* test. **F,** Bar plot represents MFI of active caspase-3 measured by flow cytometry on day 10 of exposure to TMZ (500 μmol/L) versus TMZ (500 μmol/L) + MK2206 (5 μmol/L). Data from unicate analysis of samples representing experimental (TMZ→eR; BN46) or clinical (RT/TMZ; BN118, BN123, BN132) relapse status, normalized to DMSO control. **G,** Histograms represent active caspase-3 flow cytometry data from naïve versus eR BN46 cells treated with DMSO, TMZ, and TMZ + MK2206. **H,** Bar plot representing percent ALDH1A1+/active caspase-3+ double-positive cells measured by flow cytometry at day 10, $n = 4$ samples (described in **B**), results shown as mean ± SD, *P* values calculated using the Kruskal–Wallis test followed by Dunn *post hoc* test. **I,** Graph shows percent *in vitro* cell confluence of paired naïve cells (BN46 sample) treated with 500 μmol/L TMZ (16 days), MK2206-alone (1 μmol/L, 16 days), and sequential TMZ (500 μmol/L, 16 days) → MK2206 (1 μmol/L, up to the end of assay). Data are shown as mean ± SEM (of $n = 3$ technical replicates). **J,** Kaplan–Meier plot of BN46-based orthotopic xenografts under various mono- and combination therapy schedules as shown (see Methods). $n = 5$–9 mice/group. Statistical analysis of the data is reported in Supplementary Fig. S4C. **K,** Cartoon illustrates sequential strategy to interrupt AKT-driven subclonal progression as a rational targeting paradigm.

mutational profiles in relevant PI3K–AKT pathway drivers in the investigated cohort. For an overall statement on the potential impact of molecular constellations, including the status of MGMT expression, appropriately powered translational and clinical studies are needed. Nevertheless, the dynamics of this process resembled the behavior of drug-tolerant persister cells found in response to chemotherapies and targeted anticancer agents, e.g., in melanoma, lung and colon cancer (38, 39). Drug tolerance and stem cell plasticity have already been described in glioblastoma, at least following receptor tyrosine kinase (RTK) inhibition, via epigenetically mediated Notch signaling (40). Resistance mechanisms that operate at the phenotypic level conferring resilience through adaptive plasticity represent a new theme in glioblastoma research, because this could explain why limited genetic evolution is observed at disease recurrence (9–11, 41, 42).

ALDH1A1+ cells may represent an archetype of glioma stem cells in that regard and extensive follow-up investigation could aim at characterizing the molecular machinery and the microenvironmental interactions that these cells use to resist treatment. In this study, our main concern was the therapeutic consequence of their subclonal progression, particularly considering the very limited range of clinical options at glioblastoma relapse (1, 43, 44). The most obvious choice would be the targeting of ALDH1A1 itself. There are drugs already available broadly inhibiting aldehyde dehydrogenases (e.g., disulfiram), which unfortunately can show severe side effects and toxicity (45). Isoform-specific inhibitors are under development (23), but their safety profile remain to be elucidated under the premise that ALDH1A1 is also expressed during development and in the adult brain (27, 46). We therefore approached the alternative, provided by the marked upregulation of pAKT in the target cells. Our study however lacks detailed analyses on the mechanistic links between ALDH1A1 and AKT, which may be part of a complex regulatory mechanism involving epigenetic regulation, lipid and retinol metabolism, mitochondrial function, and pleiotropic downstream effects on oncogenic signaling (23, 25, 29). We also considered, but referred for future investigation, to clarify whether re-irradiation may have a potential benefit under this constellation at glioblastoma relapse, which could have an impact on current clinical practice (47–49).

AKT is a known suppressor of apoptosis (50), and clinical-grade inhibition can be associated with improved progression-free and overall survival in advanced, pathway-altered solid tumors (51, 52). Targeting the related axis of RTK–PI3K–AKT–mTOR signaling is an ongoing matter in clinical neuro-oncology trials as well (53). AKT inhibitors can be well tolerated, but appear to remain ineffective as a monotherapy, at least in heavily pretreated patients (54). This may be attributed to the pharmacokinetic challenges of the blood-brain-barrier and CNS penetration (55), but it also could be related to the need of an adequate combinatorial treatment (56) and, as we would like to suggest here, to the additional need to stratify patients based on the dynamics of subclonal progression.

Targeting subclonal progression is not yet standard of care in glioblastoma. Our data on clinical specimens suggest that the expansion of individual subclones may be a direct consequence of a therapeutic component in the preceding treatment schedule. The cells that initiate subclonal enrichment may not be intrinsically resistant to that specific therapeutic. Thus, for the detection of aberrant subclones, analysis of recurring tumor tissue may be mandatory. As we here reveal ALDH1A1+ cells as a dynamic and TMZ-adaptive population during first-line treatment, future second-line trials would have to determine the content of ALDH1A1+/pAKT+ target cells prior to the addition of AKT inhibitors. To optimize treatment response to this dynamic and indirect targeting approach, AKT inhibition should only be initiated when the target population is considerably expanded. To determine the most appropriate time point and duration of the sequence, adaptive trial designs may be needed.

Combinatorial drug therapy is widely considered a mainstay of treatment in malignant cancers (57), and heterogeneity of driving disease mechanisms and associated targets may serve as a well-grounded basis for the choice of treatment combinations (58). Our work additionally highlights the fact that the timing of combinatorial schemes may affect the dynamics of intra-tumor subclones and via their expansion the occurrence of treatment resistance and, eventually, the course of disease. Recent evidence in a subset of malignant glioma has already exposed that concomitant vs. adjuvant TMZ schedules may impact on survival outcome (59). This further emphasizes the importance of the chronological sequence of compound combinations for rational interference with glioblastoma progression. Targeting the predictable subclonal trajectory of ALDH1A1+ cells by temporally restricted interference with AKT may be swiftly applicable to clinical practice and outperform contemporary TMZ-based treatment standards.

Authors' Disclosures

S. Kebir reports grants and personal fees from Novocure outside the submitted work. H. Fröhlich reports grants from German Federal Ministry for Science and Education during the conduct of the study. J. Matschke reports grants from Federal Ministry of Education and Research (BMBF), German Research Foundation DFG, and European Union's Framework Program for Research and Innovation Horizon 2020 (2014–2020) under Marie Skłodowska-Curie (ITN THERADNET) during the conduct of the study. V. Jendrossek reports grants from Deutsche Forschungsgemeinschaft (DFG), Federal Ministry of Education and Research, and European Commission during the conduct of the study as well as other support from Novartis Pharma AG and Lediant Biosciences Inc. outside the submitted work. B.M. Grüner reports grants from German Research Foundation — 341532333, German Research Foundation, German Cancer Aid, and German Research Foundation — 405344257 during the conduct of the study as well as grants from Federal Ministry for Economic Affairs and Energy outside the submitted work. M. Weller reports grants from Quercis and Versameb and personal fees from Novocure, Bayer, Merck (EMD), Orbus, and Philogen outside the submitted work. O. Brüstle is a cofounder and CEO of and has shares in Life & Brain GmbH; in addition, O. Brüstle is a coinventor on a patent for peripheral zone tumor cells, methods for their preparation and use issued (EP2324111; AU2009291203; US9103819). M. Glas reports personal fees from Roche, Novartis, Daiichi Sankyo, Bayer, Janssen-Cilag, Merck, Kyowa Kirin, and Seagen; grants and personal fees from Novocure; and grants from Life & Brain GmbH outside the submitted work; in addition, M. Glas has a patent for peripheral zone tumor cells, methods for their preparation and use, issued. B. Scheffler reports nonfinancial support and other support from DKTK and grants from DFG, BMBF, Bayer, and VW Foundation during the conduct of the study as well as grants from Life & Brain GmbH outside the submitted work; in addition, B. Scheffler has a patent for peripheral zone tumor cells, methods for their preparation and use issued. No disclosures were reported by the other authors.

Authors' Contributions

S. Kebir: Data curation, formal analysis, investigation, visualization, methodology, writing–original draft, writing–review and editing. **V. Ullrich:** Data curation, formal analysis, investigation, visualization, writing–review and editing. **P. Berger:** Data curation, formal analysis, investigation, visualization, writing–review and editing. **C. Dobersalske:** Data curation, formal analysis, investigation, visualization, writing–review and editing. **S. Langer:** Data curation, investigation, visualization, writing–review and editing. **L. Rauschenbach:** Formal analysis, methodology, writing–review and editing. **D. Trageser:** Investigation, writing–original draft. **A. Till:** Investigation, writing–original draft. **F.K. Lorbeer:** Data curation, investigation. **A. Wieland:** Formal analysis. **T. Wilhelm-Buchstab:** Methodology. **A. Ahmad:** Data curation. **H. Fröhlich:** Supervision, methodology. **I. Cima:** Formal analysis, writing–review and editing. **S. Prasad:** Formal analysis, methodology. **J. Matschke:** Methodology. **V. Jendrossek:** Methodology. **M. Remke:** Formal analysis. **B.M. Grüner:** Formal

analysis. **A. Roesch:** Conceptualization, formal analysis, methodology. **J.T. Siveke:** Conceptualization, formal analysis. **C. Herold-Mende:** Conceptualization, formal analysis. **T. Blau:** Data curation, formal analysis, methodology. **K. Keyvani:** Resources, formal analysis, methodology. **F.K.H. van Landeghem:** Data curation, formal analysis, methodology. **T. Pietsch:** Resources, formal analysis. **J. Felsberg:** Data curation, formal analysis, methodology. **G. Reifenberger:** Resources, formal analysis, methodology. **M. Weller:** Conceptualization, formal analysis. **U. Sure:** Conceptualization, resources. **O. Brüstle:** Conceptualization, formal analysis. **M. Simon:** Resources, methodology. **M. Glas:** Conceptualization, formal analysis, funding acquisition, methodology, writing–review and editing. **B. Scheffler:** Conceptualization, formal analysis, supervision, funding acquisition, methodology, writing–original draft, project administration, writing–review and editing.

Acknowledgments

The authors wish to thank Sabine Normann and Mihaela Keller for their assistance in cell culture work and Andreas Waha for their assistance in determining *MGMT* promoter status. Roman Reinartz, Raggu Saman, Gabor Petzold, Joao Dinis, and Emre Kocakavuk were involved in explorative studies and helped to collect preliminary data not considered for this manuscript. Rolf Fimmers has provided initial advice on the statistical evaluation of preliminary data. Cartoons and drawings generated using Servier Medical Art, provided by Servier, licensed under a Creative Commons Attribution 3.0 unported license. Composition of figures in Affinity Designer v1.10.5.

This work was supported by the German Cancer Consortium (DKTK) and funded by the Deutsche Forschungsgemeinschaft (DFG) – SCHE656/2–1, proj#418179322 and SCHE656/2–2, proj#405344257, and by a grant of the Federal Ministry of Education and Research (BMBF; FKZ03V0785). Additional grants were provided to individual investigators.

B. Scheffler: Lichtenberg program / VW Foundation, AZ82779.

I. Cima/B. Scheffler: Wilhelm Sander Stiftung (2017.148.2)

B.M. Grüner: supported by the DFG Emmy Noether program (GR4575/1–1)

J.T. Siveke: supported by the German Cancer Aid (grant no. 70112505, PIPAC; grant no. 70113834 PREDICT-PACA), the Wilhelm-Sander Foundation (grant no. 2019.008.1), the DFG through grant SI1549/3–1 (Clinical Research Unit KFO337) and SI1549/4–1, and the Federal Ministry of Education and Research (BMBF; SATURN3 consortium).

The publication costs of this article were defrayed in part by the payment of publication fees. Therefore, and solely to indicate this fact, this article is hereby marked "advertisement" in accordance with 18 USC section 1734.

Note

Supplementary data for this article are available at Clinical Cancer Research Online (http://clincancerres.aacrjournals.org/).

Received February 23, 2022; revised September 10, 2022; accepted October 7, 2022; published first October 14, 2022.

References

1. Weller M, van den Bent M, Preusser M, Le Rhun E, Tonn JC, Minniti G, et al. EANO guidelines on the diagnosis and treatment of diffuse gliomas of adulthood. Nat Rev Clin Oncol 2021;18:170–86.
2. Bhat KPL, Balasubramaniyan V, Vaillant B, Ezhilarasan R, Hummelink K, Hollingsworth F, et al. Mesenchymal differentiation mediated by NF-κB promotes radiation resistance in glioblastoma. Cancer Cell 2013;24:331–46.
3. Lee SY. Temozolomide resistance in glioblastoma multiforme. Genes Dis 2016;3:198–210.
4. Liu R, Li W, Tao B, Wang X, Yang Z, Zhang Y, et al. Tyrosine phosphorylation activates 6-phosphogluconate dehydrogenase and promotes tumor growth and radiation resistance. Nat Commun 2019;10:991.
5. Singh N, Miner A, Hennis L, Mittal S. Mechanisms of temozolomide resistance in glioblastoma - a comprehensive review. Cancer Drug Resist 2021;4:17–43.
6. Weller M, Cloughesy T, Perry JR, Wick W. Standards of care for treatment of recurrent glioblastoma–are we there yet? Neuro Oncol 2013;15:4–27.
7. Schritz A, Aouali N, Fischer A, Dessenne C, Adams R, Berchem G, et al. Systematic review and network meta-analysis of the efficacy of existing treatments for patients with recurrent glioblastoma. Neurooncol Adv 2021;3:vdab052.
8. Schafer N, Gielen GH, Rauschenbach L, Kebir S, Till A, Reinartz R, et al. Longitudinal heterogeneity in glioblastoma: moving targets in recurrent versus primary tumors. J Transl Med 2019;17:96.
9. Korber V, Yang J, Barah P, Wu Y, Stichel D, Gu Z, et al. Evolutionary trajectories of IDH (WT) glioblastomas reveal a common path of early tumorigenesis instigated years ahead of initial diagnosis. Cancer Cell 2019;35:692–704.
10. Barthel FP, Johnson KC, Varn FS, Moskalik AD, Tanner G, Kocakavuk E, et al. Longitudinal molecular trajectories of diffuse glioma in adults. Nature 2019;576:112–20.
11. Draaisma K, Chatzipli A, Taphoorn M, Kerkhof M, Weyerbrock A, Sanson M, et al. Molecular evolution of IDH wild-type glioblastomas treated with standard-of-care affects survival and design of precision medicine trials: a report from the EORTC 1542 Study. J Clin Oncol 2020;38:81–99.
12. Johnson BE, Mazor T, Hong C, Barnes M, Aihara K, McLean CY, et al. Mutational analysis reveals the origin and therapy-driven evolution of recurrent glioma. Science 2014;343:189–93.
13. Louis DN, Perry A, Wesseling P, Brat DJ, Cree IA, Figarella-Branger D, et al. The 2021 WHO classification of tumors of the central nervous system: a summary. Neuro Oncol 2021;23:1231–51.
14. Felsberg J, Wolter M, Seul H, Friedensdorf B, Goppert M, Sabel MC, et al. Rapid and sensitive assessment of the IDH1 and IDH2 mutation status in cerebral gliomas based on DNA pyrosequencing. Acta Neuropathol 2010;119:501–7.
15. Felsberg J, Rapp M, Loeser S, Fimmers R, Stummer W, Goeppert M, et al. Prognostic significance of molecular markers and extent of resection in primary glioblastoma patients. Clin Cancer Res 2009;15:6683–93.
16. Mikeska T, Bock C, El-Maarri O, Hubner A, Ehrentraut D, Schramm J, et al. Optimization of quantitative MGMT promoter methylation analysis using pyrosequencing and combined bisulfite restriction analysis. J Mol Diagn 2007;9:368–81.
17. Schaefer MH, Fontaine JF, Vinayagam A, Porras P, Wanker EE, Andrade-Navarro MA. HIPPIE: Integrating protein interaction networks with experiment based quality scores. PLoS One 2012;7:e31826.
18. Jiang H, Lei R, Ding SW, Zhu S. Skewer: a fast and accurate adapter trimmer for next-generation sequencing paired-end reads. BMC Bioinf 2014;15:182.
19. Remmele W, Hildebrand U, Hienz HA, Klein PJ, Vierbuchen M, Behnken LJ, et al. Comparative histological, histochemical, immunohistochemical, and biochemical studies on estrogen receptors, lectin receptors, and Barr bodies in human breast cancer. Virchows Arch A Pathol Anat Histopathol 1986;409:127–47.
20. Glas M, Rath BH, Simon M, Reinartz R, Schramme A, Trageser D, et al. Residual tumor cells are unique cellular targets in glioblastoma. Ann Neurol 2010;68:264–9.
21. Scheffler B, Walton NM, Lin DD, Goetz AK, Enikolopov G, Roper SN, et al. Phenotypic and functional characterization of adult brain neuropoiesis. Proc Natl Acad Sci U S A 2005;102:9353–8.
22. Reinartz R, Wang S, Kebir S, Silver DJ, Wieland A, Zheng T, et al. Functional subclone profiling for prediction of treatment-induced intra-tumor population shifts and discovery of rational drug combinations in human glioblastoma. Clin Cancer Res 2017;23:562–74.
23. Yue H, Hu Z, Hu R, Guo Z, Zheng Y, Wang Y, et al. ALDH1A1 in cancers: bidirectional function, drug resistance, and regulatory mechanism. Front Oncol 2022;12:918778.
24. Levi BP, Yilmaz OH, Duester G, Morrison SJ. Aldehyde dehydrogenase 1a1 is dispensable for stem cell function in the mouse hematopoietic and nervous systems. Blood 2009;113:1670–80.
25. Schafer A, Teufel J, Ringel F, Bettstetter M, Hoepner I, Rasper M, et al. Aldehyde dehydrogenase 1A1–a new mediator of resistance to temozolomide in glioblastoma. Neuro Oncol 2012;14:1452–64.
26. Campos B, Centner FS, Bermejo JL, Ali R, Dorsch K, Wan F, et al. Aberrant expression of retinoic acid signaling molecules influences patient survival in astrocytic gliomas. Am J Pathol 2011;178:1953–64.
27. Adam SA, Schnell O, Poschl J, Eigenbrod S, Kretzschmar HA, Tonn JC, et al. ALDH1A1 is a marker of astrocytic differentiation during brain development and correlates with better survival in glioblastoma patients. Brain Pathol 2012;22:788–97.

28. Wang Z, Zhang H, Xu S, Liu Z, Cheng Q. The adaptive transition of glioblastoma stem cells and its implications on treatments. Signal Transduct Target Ther 2021; 6:124.
29. McKinney A, Lindberg OR, Engler JR, Chen KY, Kumar A, Gong H, et al. Mechanisms of resistance to EGFR inhibition reveal metabolic vulnerabilities in human GBM. Mol Cancer Ther 2019;18:1565–76.
30. Riemenschneider MJ, Betensky RA, Pasedag SM, Louis DN. AKT activation in human glioblastomas enhances proliferation via TSC2 and S6 kinase signaling. Cancer Res 2006;66:5618–23.
31. Majewska E, Szeliga M. AKT/GSK3β signaling in glioblastoma. Neurochem Res 2017;42:918–24.
32. Hambardzumyan D, Squatrito M, Carbajal E, Holland EC. Glioma formation, cancer stem cells, and akt signaling. Stem Cell Rev 2008;4:203–10.
33. Eyler CE, Foo WC, LaFiura KM, McLendon RE, Hjelmeland AB, Rich JN. Brain cancer stem cells display preferential sensitivity to Akt inhibition. Stem Cells 2008;26:3027–36.
34. Janku F, Meric-Bernstam F. Targeting the PI3K pathway in cancer: Are we making headway? Nat Rev Clin Oncol 2018;15:273–91.
35. Porter AG, Janicke RU. Emerging roles of caspase-3 in apoptosis. Cell Death Differ 1999;6:99–104.
36. Bao S, Wu Q, McLendon RE, Hao Y, Shi Q, Hjelmeland AB, et al. Glioma stem cells promote radioresistance by preferential activation of the DNA damage response. Nature 2006;444:756–60.
37. Chen J, Li Y, Yu TS, McKay RM, Burns DK, Kernie SG, et al. A restricted cell population propagates glioblastoma growth after chemotherapy. Nature 2012; 488:522–6.
38. Marine JC, Dawson SJ, Dawson MA. Nongenetic mechanisms of therapeutic resistance in cancer. Nat Rev Cancer 2020;20:743–56.
39. Rehman SK, O'Brien CA. Persister cells that survive chemotherapy are pinpointed. Nature 2022;608:675–6.
40. Liau BB, Sievers C, Donohue LK, Gillespie SM, Flavahan WA, Miller TE, et al. Adaptive chromatin remodeling drives glioblastoma stem cell plasticity and drug tolerance. Cell Stem Cell 2017;20:233–46.
41. Yabo YA, Niclou SP, Golebiewska A. Cancer cell heterogeneity and plasticity: a paradigm shift in glioblastoma. Neuro Oncol 2022;24:669–82.
42. Gimple RC, Yang K, Halbert ME, Agnihotri S, Rich JN. Brain cancer stem cells: resilience through adaptive plasticity and hierarchical heterogeneity. Nat Rev Cancer 2022;22:497–514.
43. Lau D, Magill ST, Aghi MK. Molecularly targeted therapies for recurrent glioblastoma: current and future targets. Neurosurg Focus 2014;37:E15.
44. Lazaridis L, Schmidt T, Oster C, Blau T, Pierscianek D, Siveke JT, et al. Precision neuro-oncology: a pilot analysis of personalized treatment in recurrent glioma. J Cancer Res Clin Oncol 2022.
45. De Sousa A. Disulfiram: side effects and toxicity. In: Disulfiram. Singapore: Springer; 2019. https://doi.org/10.1007/978–981–32–9876–7_7.
46. Anderson DW, Schray RC, Duester G, Schneider JS. Functional significance of aldehyde dehydrogenase ALDH1A1 to the nigrostriatal dopamine system. Brain Res 2011;1408:81–7.
47. Mehta M, Khan A, Danish S, Haffty BG, Sabaawy HE. Radiosensitization of primary human glioblastoma stem-like cells with low-dose AKT inhibition. Mol Cancer Ther 2015;14:1171–80.
48. Djuzenova CS, Fiedler V, Memmel S, Katzer A, Sisario D, Brosch PK, et al. Differential effects of the Akt inhibitor MK-2206 on migration and radiation sensitivity of glioblastoma cells. BMC Cancer 2019;19:299.
49. Minniti G, Niyazi M, Alongi F, Navarria P, Belka C. Current status and recent advances in re-irradiation of glioblastoma. Radiat Oncol 2021;16: 36.
50. Franke TF, Hornik CP, Segev L, Shostak GA, Sugimoto C. PI3K/Akt and apoptosis: size matters. Oncogene 2003;22:8983–98.
51. Hyman DM, Smyth LM, Donoghue MTA, Westin SN, Bedard PL, Dean EJ, et al. AKT inhibition in solid tumors with AKT1 mutations. J Clin Oncol 2017;35: 2251–9.
52. Howell SJ, Casbard A, Carucci M, Ingarfield K, Butler R, Morgan S, et al. Fulvestrant plus capivasertib versus placebo after relapse or progression on an aromatase inhibitor in metastatic, estrogen receptor-positive, HER2-negative breast cancer (FAKTION): overall survival, updated progression-free survival, and expanded biomarker analysis from a randomized, phase II trial. Lancet Oncol 2022;23:851–64.
53. Colardo M, Segatto M, Di Bartolomeo S. Targeting RTK–PI3K–mTOR axis in gliomas: an update. Int J Mol Sci 2021;22.
54. Kaley TJ, Panageas KS, Mellinghoff IK, Nolan C, Gavrilovic IT, DeAngelis LM, et al. Phase II trial of an AKT inhibitor (perifosine) for recurrent glioblastoma. J Neurooncol 2019;144:403–7.
55. Cole DE, Lester-McCully CM, Widemann BC, Warren KE. Plasma and cerebrospinal fluid pharmacokinetics of the Akt inhibitor, perifosine, in a nonhuman primate model. Cancer Chemother Pharmacol 2015;75: 923–8.
56. Kaley TJ, Panageas KS, Pentsova EI, Mellinghoff IK, Nolan C, Gavrilovic I, et al. Phase I clinical trial of temsirolimus and perifosine for recurrent glioblastoma. Ann Clin Transl Neurol 2020;7:429–36.
57. Al-Lazikani B, Banerji U, Workman P. Combinatorial drug therapy for cancer in the post-genomic era. Nat Biotechnol 2012;30:679–92.
58. Reifenberger G, Wirsching HG, Knobbe-Thomsen CB, Weller M. Advances in the molecular genetics of gliomas—implications for classification and therapy. Nat Rev Clin Oncol 2017;14:434–52.
59. van den Bent MJ, Tesileanu CMS, Wick W, Sanson M, Brandes AA, Clement PM, et al. Adjuvant and concurrent temozolomide for 1p/19q non-co-deleted anaplastic glioma (CATNON; EORTC study 26053–22054): second interim analysis of a randomized, open-label, phase III study. Lancet Oncol 2021;22: 813–23.